research papers





Received 15 July 2022 Accepted 20 September 2022

Edited by L. Dawe, Wilfrid Laurier University, Waterloo, Ontario, Canada

Keywords: crystal structure; C—H hydrogen bonding; halogen bond; halogen—halogen interaction; self-complementary halogen bond; bifurcated C—H···nitro hydrogen bond; Hirshfeld surface; intermolecular energy; energy frameworks.

CCDC references: 2208447; 2208446; 2208445

Supporting information: this article has supporting information at journals.iucr.org/c

A structural and computational comparison of close contacts and related intermolecular energies of interaction in the structures of 1,3-diiodo-5-nitrobenzene, 1,3-dibromo-5-nitrobenzene, and 1,3-di-chloro-5-nitrobenzene

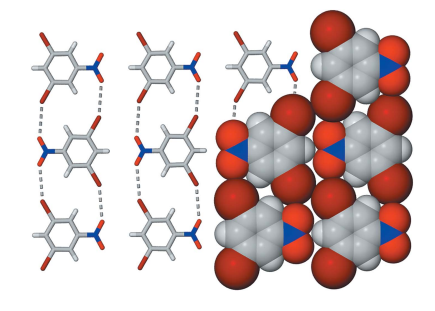
Eric Bosch, a* Nathan P. Bowling and Erin D. Speetzen

^aDepartment of Chemistry and Biochemistry, Missouri State University, 901 South National Avenue, Springfield, MO 65897, USA, and ^bDepartment of Chemistry, University of Wisconsin-Stevens Point, 2101 Fourth Avenue, Stevens Point, WI 54481, USA. *Correspondence e-mail: ericbosch@missouristate.edu

1,3-Diiodo-5-nitrobenzene, $C_6H_3I_2NO_2$, and 1,3-dibromo-5-nitrobenzene, C_6H_3 -Br $_2NO_2$, crystallize in the centrosymmetric space group $P2_1/m$, and are isostructural with 1,3-dichloro-5-nitrobenzene, $C_6H_3Cl_2NO_2$, that has been redetermined at 100 K for consistency. While the three-dimensional packing in all three structures is similar, the size of the halogen atom affects the nonbonded close contacts observed between molecules. Thus, the structure of 1,3-diiodo-5-nitrobenzene features a close Type 1 I \cdots I contact, the structure of 1,3-dibromo-5-nitrobenzene features a self-complementary nitro-O \cdots Br close contact, while the structure of 1,3-dichloro-5-nitrobenzene also has a self-complementary nitro-O \cdots Cl interaction, as well as a bifurcated $C-H\cdots$ O(nitro) close contact. Notably, the major energetically attractive intermolecular interaction between adjacent molecules in each of the three structures corresponds to a π -stacked interaction. The self-complementary halogen \cdots O(nitro) and $C-H\cdots$ O(nitro) interactions correspond to significant cohesive attraction between molecules in each structure, while the Type 1 halogen–halogen contact is weakly cohesive.

1. Introduction

Iodo and nitro substituents on aromatic rings are versatile groups that facilitate the synthesis of a wide variety of molecules. Iodoarenes are reactive in a variety of transition-metalcatalysed cross coupling reactions, including the Heck and Sonogashira coupling reactions, while the nitro substituent can be transformed into a variety of other substituents following reduction and diazotization. Recently, 1,3-diiodo-5-nitrobenzene, (1), has been used as a key intermediate in a variety of studies, including the self-assembly of porphyrin-based supramolecular systems (van der Weegen et al., 2017), the organogelation of halogen-functionalized dendrons (Feng et al., 2016), and the formation of redox-active ferrocene derivatives (Lim et al., 2015). Earlier, we prepared 1,3-diiodo-5nitrobenzene as an intermediate with a view to preparing substituted electron-poor polyphenylethynylenes, an ongoing area of interest. We were intrigued by the potential interplay between intermolecular halogen-halogen interactions and halogen-nitro interactions within the structure of this compound, (1), and the dihalo analogues 1,3-dibromo-5-nitrobenzene, (2), and 1,3-dichloro-5-nitrobenzene, (3) (Scheme 1). The goal of the study is to compare, and contrast, the close intermolecular contacts and the related intermolecular energies of interaction within each structure.



s20532296, 2022, 10, Downloaded from https://onlinelibrary.wiey.com/doi/10.1107/S2053229622009275 by University Of Wisconsin - Sp. Wiley Online Library on [26/10/2023]. See the Terms and Conditions (https://onlinelibrary.wiley.com/term

For all structures: monoclinic, $P2_1/m$, Z = 2. Experiments were carried out at 100 K with Mo $K\alpha$ radiation using a Bruker APEX-I CCD diffractometer. Absorption was corrected for by multi-scan methods (SADABS; Bruker, 2014). Refinement was on 55 parameters. H-atom parameters were constrained.

	(1)	(2)	(3)
Crystal data			
Chemical formula	$C_6H_3I_2NO_2$	$C_6H_3Br_2NO_2$	C ₆ H ₃ Cl ₂ NO ₂
$M_{ m r}$	374.89	280.91	191.99
a, b, c (Å)	4.1810 (5), 15.0336 (17), 6.7970 (8)	3.9721 (7), 14.164 (2), 6.7971 (11)	3.8115 (3), 13.6452 (11), 6.8976 (5)
β (°)	96.506 (2)	96.486 (2)	94.632 (1)
$V(\mathring{A}^3)$	424.48 (9)	379.97 (11)	357.56 (5)
$\mu \text{ (mm}^{-1})$	7.36	10.61	0.85
Crystal size (mm)	$0.20 \times 0.20 \times 0.20$	$0.38 \times 0.26 \times 0.09$	$0.37 \times 0.13 \times 0.03$
Data collection			
T_{\min} , T_{\max}	0.406, 0.746	0.343, 0.746	0.702, 0.746
No. of measured, independent and observed $[I > 2\sigma(I)]$ reflections	5377, 982, 974	4446, 874, 764	4560, 813, 747
$R_{\rm int}$	0.019	0.044	0.021
$(\sin \theta/\lambda)_{\max} (\mathring{A}^{-1})$	0.643	0.642	0.640
Refinement			
$R[F^2 > 2\sigma(F^2)], wR(F^2), S$	0.019, 0.040, 1.35	0.029, 0.081, 1.09	0.028, 0.071, 1.12
No. of reflections	982	874	813
$\Delta \rho_{\rm max}, \Delta \rho_{\rm min} ({ m e \ \AA}^{-3})$	0.77, -0.75	1.04, -0.52	0.37, -0.22

Computer programs: SMART (Bruker, 2014), SAINT (Bruker, 2014), SHELXT2018 (Sheldrick, 2015a), SHELXL2018 (Sheldrick, 2015b), and X-SEED (Barbour, 2020).

The study of noncovalent interactions has led to the description of reliable supramolecular motifs that facilitate the directed preparation of supramolecular systems. Supramolecular synthons related to intermolecular interactions involving nitro groups and halogens are established. Key to this development has been the recognition of the σ -hole on halogen atoms bonded to carbon or nitrogen (Politzer & Murray, 2013). The σ -hole is most pronounced on iodine and is further amplified by the neighboring attachment of electronwithdrawing atoms, especially fluorine (Clark et al., 2007), or electron-withdrawing groups like the nitro group (Nguyen et al., 2016). The σ -hole interacts with a Lewis base, typically to an N or O atom, to form a near-linear halogen bond [Fig. 1(a)]. Halogen bonds to a nitro group include the symmetric bifurcated nitro-halogen supramolecular synthon [Fig. 1(b)] (Thalladi et al., 1996; Nemec & Cinčić, 2016), an asymmetric bifurcated interaction [Fig. 1(c)], and a halogen bond to one O atom [Fig. 1(d)], where the nitro and halogen-bonded C atoms are *cis* relative to the N-O $\cdots X$ group (Allen *et al.*, 1997).

Halogen-halogen interactions are characterized according to the molecular geometry of the two C-X groups, as shown in Fig. 2. Thus, the offset head-to-head Type I contacts have $\theta 1 \simeq \theta 2$, while Type II contacts have $\theta 1 \simeq 90^\circ$ and $\theta 2 \simeq 180^\circ$. The largely dispersive Type I interactions are often symmetrical, either *trans* as shown or *cis*, with an energy minimum at $\theta 1 \simeq \theta 2 \simeq 150^\circ$ (Ramasubbu *et al.*, 1986; Awwadi *et al.*, 2006). The Type II contacts maximize the electrostatic interaction

based on the asymmetric charge distribution on bound halogen atoms. Type III interactions are defined as the subset of interactions with $\theta 1 \simeq \theta 2 \simeq 180^\circ$ (Ibrahim & Moussa, 2020), while Type IV interactions are defined as the subset of interactions with $\theta 1 \simeq \theta 2 \simeq 90^\circ$ (Ibrahim *et al.*, 2022).

Traditionally, the role and importance of close contacts have been reported and evaluated based on the comparison of the measured interatomic distances as compared to the corresponding sum of the van der Waals radii. These close contacts, less than the sum of the van der Waals radii, are now readily visualized and investigated using the Hirshfeld surface (Spackman & Jayatilaka, 2009) of a molecule within its crystalline environment using the program *CrystalExplorer* (Spackman *et al.*, 2021). It is intuitively reasonable that close contacts are not necessarily cohesive. Consequently, the application of programs like *CrystalExplorer* to calculate intermolecular interaction energies within the crystal structure provide a useful supplementary tool to evaluate these interactions (Turner *et al.*, 2014). The intermolecular energies of interaction are often displayed visually as energy frameworks

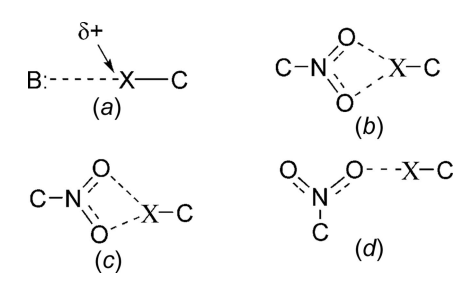


Figure 1 (a) Generic halogen-bond motif between a carbon-bound halogen and a Lewis base; (b) symmetric bifurcated halogen \cdots O(nitro) interaction; (c) asymmetric bifurcated halogen \cdots O(nitro) interaction; (d) isolated halogen \cdots O(nitro) bond.

and-conditions) on Wiley Online Library for rules of use; OA articles are governed by the applicable Creative Commons Licens

Figure 2
(a) Type I halogen-halogen interaction and (b) Type II halogen-halogen interaction

(Mackenzie *et al.*, 2017). Provided that the contact between two molecules in the solid state mainly corresponds to the observed close contact between those molecules, then it is reasonable to correlate the close contact to the energy of interaction between those molecules. The goal of this study is then to combine these two features of *CrystalExplorer* to further evaluate the role, or importance, of close contacts in the analysis of the self-complementary halogen \cdots O(nitro), C—H \cdots O(nitro), and Type 1 halogen—halogen intermolecular interactions as compared to π -stacking within the three analogous 1,3-dihalo-5-nitrobenzenes.

2. Experimental

2.1. Materials and crystallization

1,3-Diiodo-5-nitrobenzene was available from a previous unpublished study and the spectral data are identical to those reported in the literature (Bérubé & Poirier, 2004). 1,3-Dibromo-5-nitrobenzene and 1,3-dichloro-5-nitrobenzene are commercially available and were used as received. All three compounds are colorless white solids. 0.025 g of each of the dihalonitrobenzenes was dissolved in 2 ml of chloroform in a 5 ml screw cap vial. The vial was loosely capped, set aside, and the solvent allowed to evaporate slowly. This yielded a homogeneous mass of crystals suitable for single-crystal X-ray analysis.

2.2. Refinement

Crystal data, data collection and structure refinement details are summarized in Table 1. The aromatic H atoms, which were all observed in difference maps, were treated as riding atoms in geometrically idealized positions, with C-H=0.95~Å (aromatic) and $U_{\rm iso}(H)=1.2U_{\rm eq}(C)$. The structure of (3) has been reported at room temperature (Bhar *et al.*, 1995)

and at 100 K (Guillot, 2019). The structure reported here is essentially identical to that previously reported at 100 K.

2.3. Calculations

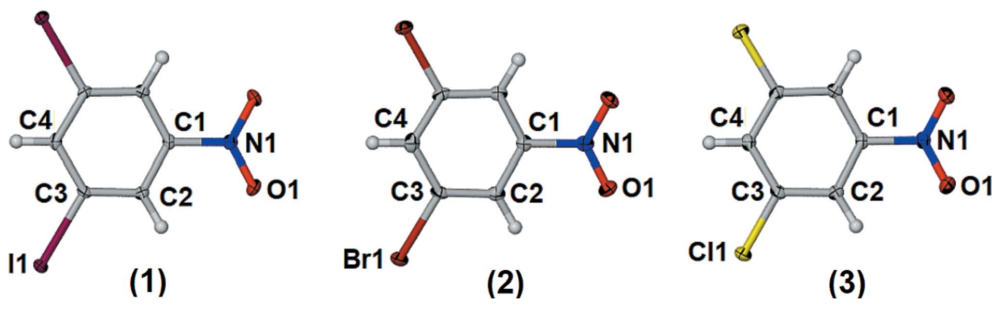
The molecular electrostatic potential energy surfaces were calculated using Spartan'10 (Wavefunction, 2010). The molecules of (1), (2), and (3) were geometry optimized and the molecular electrostatic potential calculated using density functional theory (DFT) at the B3LYP/6-311+G** level. The program CrystalExplorer (Version 17; Turner et al., 2017) was used to calculate the Hirshfeld surface, as well as the intermolecular interaction energies within each crystal structure. In addition to calculating the interaction energies between pairs of molecules in the crystal, CrystalExplorer also decomposes the interaction energy into four physically motivated terms: (i) the classical electrostatic energy (E_{elec}) , (ii) the polarization energy (E_{pol}) , (iii) the dispersion energy (E_{dis}) , and (iv) the exchange-repulsion energy (E_{rep}) (Turner et al., 2014; Mackenzie et al., 2017). The breakdown of the interaction energies is collated in Tables S1–S3 (see supporting information).

3. Results and discussion

3.1. Crystallographic analysis

Compound (1) crystallizes in the centrosymmetric space group $P2_1/m$ and the asymmetric unit is one half of (1), which lies on a crystallographic mirror plane along the C-N bond and perpendicular to the plane of the arene ring. Compounds (2) and (3) also crystallize in the space group $P2_1/m$. The asymmetric unit of each of these are shown in Fig. 3 with the symmetry-generated second half of the molecules.

In the crystal structure of (1), the molecules are arranged head-to-tail in linear ribbons with adjacent ribbons tail-to-head to form sheets as shown in Fig. 4. There is a Type I halogen-halogen interaction, with an $I1\cdots I1^i$ separation of 3.7599 (5) Å and a $C-I\cdots I^i$ angle of 144.01 (9)° [symmetry code: (i) -x+2, -y+1, -z] between adjacent I atoms; see **A** in Fig. 4. The $I\cdots I$ separation is 94.9% of the sum of the van der Waals radii (Bondi, 1964). The second close contact, **B** in Fig. 4, is a self-complementary interaction between the I atom and a nitro O atom, with an $I1\cdots O1^{ii}$ separation of 3.492 (3) Å and a $C-I\cdots O^{ii}$ angle of 152.31 (10)° [symmetry code: (ii) -x+1, -y+1, -z+1]. The $I\cdots O$ distance is similar to the sum of the van der Waals radii of 3.50 Å. These angles and



The molecular structures of (1), (2), and (3), with the atom labeling. Displacement ellipsoids are drawn at the 50% probability level.

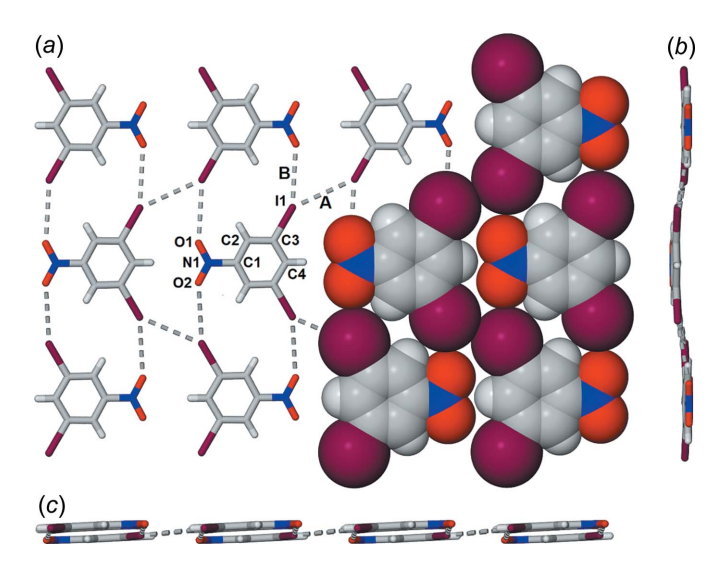
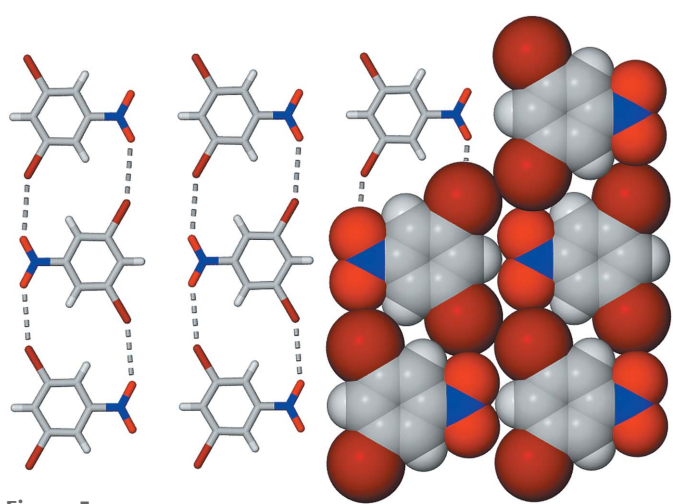


Figure 4 (a) View of a planar sheet of molecules (1), with close $I \cdots I$ and $I \cdots O$ contacts shown as dashed grey lines, labeled **A** and **B**, respectively, and emphasized with a partial space-filling model. The two mutually orthogonal views are shown as parts (b) and (c).

distances thus lie in the range of weak halogen bonds to iodine with an O-atom acceptor (see Fig. S1 for a scatterplot of halobenzene halogen bonds to oxygen). Accordingly, this should be considered a self-complementary weak halogen bond to oxygen. The planar sheets are slightly corrugated, as shown in views (b) and (c) in Fig. 4. The molecules of (1) are offset π -stacked, with a centroid-to-centroid distance of 4.181 (2) Å and a perpendicular distance between molecules of 3.4911 (16) Å.

The overall packing of the dibromo compound (2) is similar to that of (1), as shown in Fig. 5. In the structure of (2), the closest intermolecular contact is a self-complementary $\text{Br}\cdots\text{O}$ halogen bond, with a $\text{Br}1\cdots\text{O}1^i$ separation of 3.257 (3) Å and a $\text{C3-Br}1\cdots\text{O}^i$ angle of 151.33 (11)° [symmetry code: (i) -x+1, -y+1, -z+1]. The $\text{Br}\cdots\text{O}$ separation, 96.6% of the



View of a planar sheet of molecules of (2), with close Br···O contacts shown as dashed grey lines and emphasized with a partial space-filling model.

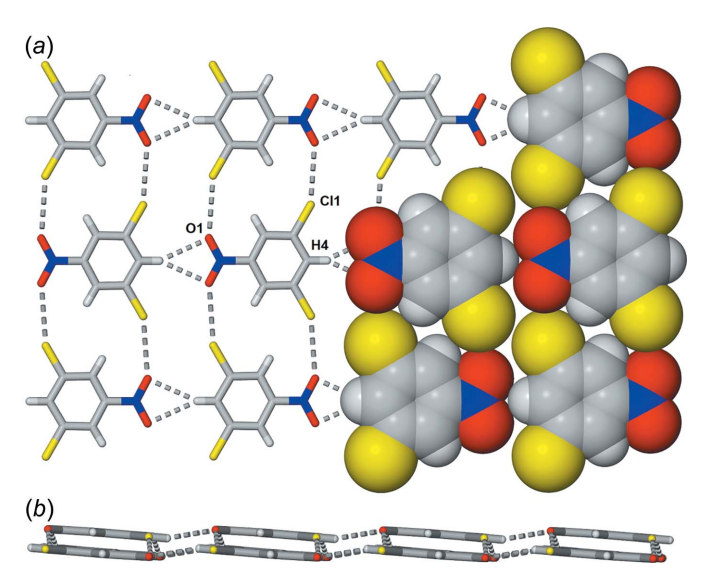


Figure 6 (a) View of a sheet of molecules of (3), with close $Cl \cdots O$ and bifurcated $NO_2 \cdots H$ contacts shown as dashed grey lines and emphasized with a partial space-filling model. (b) Orthogonal view showing the offset arrangement of alternate ribbons of (3) within the plane.

sum of the van der Waals interaction, is shown as dashed lines in Fig. 5. The bromine–bromine separation of 3.7048 (8) Å is essentially the same as the sum of the van der Waals radii of 3.70 Å. The offset π -stacked molecules have a centroid-to-centroid distance of 3.972 (2) Å and a perpendicular distance between molecules of 3.3990 (16) Å.

In the structure of (3), there are two intermolecular contacts less than the sum of the van der Waals radii. One of these is the self-complementary $Cl\cdots O$ interaction, like that shown for (1) and (2). The other is a bifurcated nonconventional $C-H\cdots O(nitro)$ hydrogen bond, as shown in Fig. 6.

The self-complementary Cl···O halogen bond has a Cl1···O1ⁱ separation of 3.2029 (12) Å and a C3-Cl1···O1ⁱ angle of 150.47 (6)° [symmetry code: (i) -x + 1, -y + 1, -z + 1], while the bifurcated C-H···O interaction has a H4···O1ii separation of 2.6717 Å and a C4-H4···O1ⁱⁱ angle of 152.38° [symmetry code: (ii) x + 1, y, z - 1]. This close $C-H \cdots O$ interaction is presumably favored for the chloro derivative (3) as opposed to (1) and (2) due to the smaller size of the Cl atom. For comparison, the C4···O1ⁱⁱ distance is 3.541 (2) Å in (3) as compared to 4.075 and for 4.151 Å for (2) and (1), respectively. The Cl···O separation is 98% of the sum of the van der Waals radii, while the Cl···Cl separation of 3.752 (2) Å is significantly longer than the sum of the van der Waals radii of 3.50 Å. The centroid-to-centroid distance between offset π -stacked molecules is 3.8115 (10) Å, with a perpendicular distance between molecules of 3.3710 (7) Å.

3.2. Molecular electrostatic potentials

The head-to-tail arrangement within each strand of molecules was confirmed to be electrostatic by calculation of the molecular electrostatic potential plots shown in Fig. 7. The primary areas of negative potential lie on the nitro O atoms in

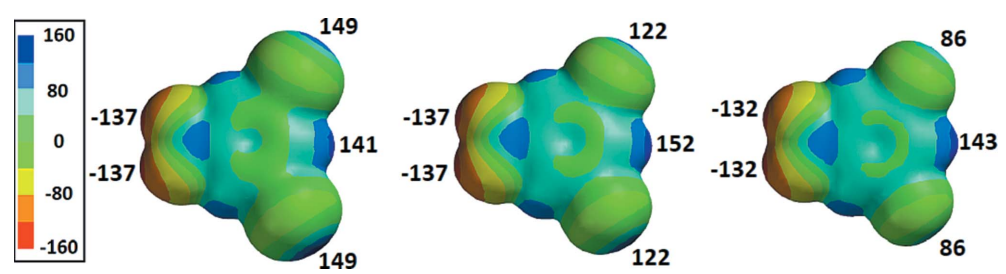


Figure 7 Molecular electrostatic potential maps of (1), (2), and (3) from left to right shown with the same potential range scale from -160 to 160 kJ mol⁻¹ and with the calculated maxima and minima for each annotated in kJ mol⁻¹.

all three molecules, while the positive potential resides on the halogen atoms and the H atom between the halogens. As expected, the electrostatic potential at the end of the C-X bonds, referred to as the σ -hole in halogen bonding, decreases from iodine to chlorine and the positive electrostatic potential on the arene H atom *ortho* to both halogen atoms and the nitro O atoms is relatively unchanged.

3.3. Hirshfeld surface and intermolecular interaction energy analysis

The Hirshfeld surface providing a visual interpretation of the intermolecular close contacts was coupled with the intermolecular energies of interaction of molecules in close contact to determine the effective role of the close contacts within each structure. The Hirshfeld surface of (1) shows that the $I \cdots I$ contact is the closest, while the $I \cdots O$ interaction is also visible as a less intense red area on the Hirshfeld surface (Fig. 8). The intermolecular energy of interaction was calculated for the six unique adjacent molecules within 4.2 Å of the central molecule of (1). Fig. 8 shows each of the unique interacting molecules color coded.

The strongest intermolecular interaction is between offset π -stacked molecules represented by the dark-blue molecule in Fig. 8, with a total intermolecular energy of -31.5 kJ mol⁻¹ largely due to a dominant dispersion component ($E_{\rm dis} = -49.9$ kJ mol⁻¹). The adjacent molecule with a self-complementary $O \cdots I$ interaction (red in Fig. 8) has the second most

Figure 8
Oblique view of the six unique molecules, color coded, closest to the central molecule of (1), which is shown with the Hirshfeld surface. Red highlights on the Hirshfeld surface indicate close contacts.

attractive interaction with a total energy of interaction of $-19.0~\rm kJ~mol^{-1}$ (Table S1). The major contributions to this are electrostatic and dispersion, with a significant repulsive contribution. The head-to-tail bifurcated C—H···O(nitro) interacting molecule (light blue in Fig. 8) has a total energy of interaction of $-12.0~\rm kJ~mol^{-1}$. In contrast, and despite the close I···I contact, the molecule interacting primarily through the Type I halogen–halogen interaction (green in Fig. 8) has an $E_{\rm tot}$ of $-0.7~\rm kJ~mol^{-1}$, where the repulsive component ($E_{\rm rep}$ = $28.7~\rm kJ~mol^{-1}$) dominates the electrostatic and dispersion interaction energies (Table S1). This highlights the importance of coupling close-contact data with intermolecular energy calculations since, in this structure, the I···I interaction is clearly the closest contact, but overall, a weakly cohesive interaction within the crystal.

The Hirshfeld surface and intermolecular interaction energies corresponding to the six unique molecules within 3.80 Å of the central molecule of (2) were calculated and Fig. 9 shows the Hirshfeld surface and the six color-coded interacting molecules. The only significant red coloration on the Hirshfeld surface corresponds to the self-complementary $\text{Br}\cdots\text{O}$ contact.

The most significant intermolecular interaction in (2) is again the π -stacked molecule (light blue in Fig. 9), with a similar total interaction energy of $-29.0 \text{ kJ mol}^{-1}$ (Table S2). The yellow molecule interacting through the self-complementary Br \cdots O halogen bond molecules has the second most attractive interaction, with an interaction energy of $-15.2 \text{ kJ mol}^{-1}$, and has significant electrostatic and dispersion contributions. The bifurcated $C-H\cdots O(\text{nitro})$ interaction has an overall interaction energy of $-10.8 \text{ kJ mol}^{-1}$.

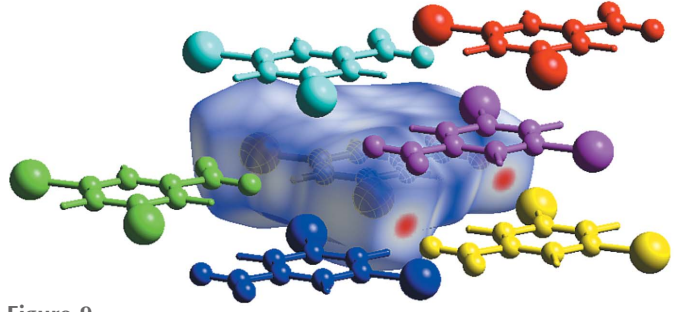


Figure 9
Oblique view of the six unique molecules, color coded, closest to the central molecule of (2), which is shown with the Hirshfeld surface.

\$20532296, 2022, 10, Downloaded from https://onlinelibrary.wiley.com/doi/10.1107/S2053229622009275 by University Of Wisconsin - Sp, Wiley Online Library on [26/10/2023]. See the Terms and Conditions (https://onlinelibrary.wiley.com/terms/

Table 2 Intermolecular energies of interaction, in kJ mol⁻¹, for molecules within 3.8 Å of (1), (2), and (3), as related to the intermolecular interaction within each pair of interacting molecules.

Major interaction with $X = \text{halogen}$	X = I	X = Br	X = Cl
π - π stacking (perpendicular π - π) ^a	-31.5 (3.4909)	-29.0 (3.3990)	-23.6 (3.3710)
Self-complementary $X \cdots O(X \cdots O)^b$	$-19.0\ (3.492)$	-15.2 (3.257)	$-9.1\ (3.2029)$
Bifurcated $C-H\cdots O (H\cdots O)^b$	-12.0(2.844)	-10.8(2.759)	-10.9(2.6717)
Type I $X \cdots X (X \cdots X)^b$	-0.7(3.7599)	-3.3 (3.7048)	-1.7(3.752)

Notes: (a) perpendicular π - π separation in Å; (b) separation between interacting atoms in Å.

The total interaction energy of the dark-blue molecule with a bromine-bromine Type I interaction is -3.3 kJ mol^{-1} .

The Hirshfeld surface of (3) and the six unique molecules within 3.80 Å of the central molecule are shown in Fig. 10. The Hirshfeld surface clearly shows the two closest contacts as the bifurcated $C-H\cdots O$ interaction with the light-blue molecule and the self-complementary $Cl\cdots O$ interaction with the red molecule. As observed with (1) and (2), the π -stacked molecule (pink in Fig. 10) has the strongest energy of interaction, with an E_{tot} value of -23.6 kJ mol $^{-1}$ (Table S3). The molecule corresponding to the bifurcated $C-H\cdots O$ interaction (light blue) has the second strongest interaction energy, with $E_{tot} = -10.9$ kJ mol $^{-1}$, and the molecule corresponding to the self-complementary $Cl\cdots O$ interaction (red) has an E_{tot} value of -9.1 kJ mol $^{-1}$. The interaction energy of the molecule with a chlorine–chlorine Type I interaction (green in Fig. 10) is -1.7 kJ mol $^{-1}$.

For comparison, the intermolecular interaction energies corresponding to the prominent close contacts are collated in Table 2. While the table contains all the relevant numerical data for the intermolecular energies of interaction for the compounds, an energy framework diagram can be used to visualize the key interactions. The energy framework for (3) is shown in Fig. 11, where the view along the c axis [Fig. 11(a)] features thicker tubes parallel to the a axis corresponding to the dominant π -stacking interaction. The secondary cohesive interactions correlated with the self-complementary halogenoxygen interaction and the bifurcated $C-H\cdots O(nitro)$ interaction are best viewed along the a axis, as shown in Fig. 11(b).

A search of the Cambridge Structural Database (Version 5.41; Groom et al., 2016) using ConQuest (Version 2020.2.0;

Figure 10 Oblique view of the six unique molecules, color coded, closest to the central molecule of (3), which is shown with the Hirshfeld surface. The red highlights on the Hirshfeld surface correspond to the two bifurcated $C-H\cdots O$ and $Cl\cdots O$ close contacts.

Bruno *et al.*, 2002) for the self-complementary halogen \cdots O(nitro) interactions where both halogen \cdots O(nitro) distances are equal to, or less than, the sum of the van der Waals radii, as shown in Fig. 12(a), yielded 44 hits with a total of 46 interactions. A similar search for *m*-halo nitrobenzenes yielded 688 hits, suggesting that this is a relatively uncommon synthon. A search for structures containing the bifurcated arene–nitrobenzene $C-H\cdots O$ interaction, as shown in Fig. 12(b), with $H\cdots O$ distances less than or equal to the sum of the van der Waals radii and $C-H\cdots N$ angles from 135 to 180°, yielded 346 instances in 329 structures. With less restrictive $H\cdots O$ distances less than or equal to the sum of the

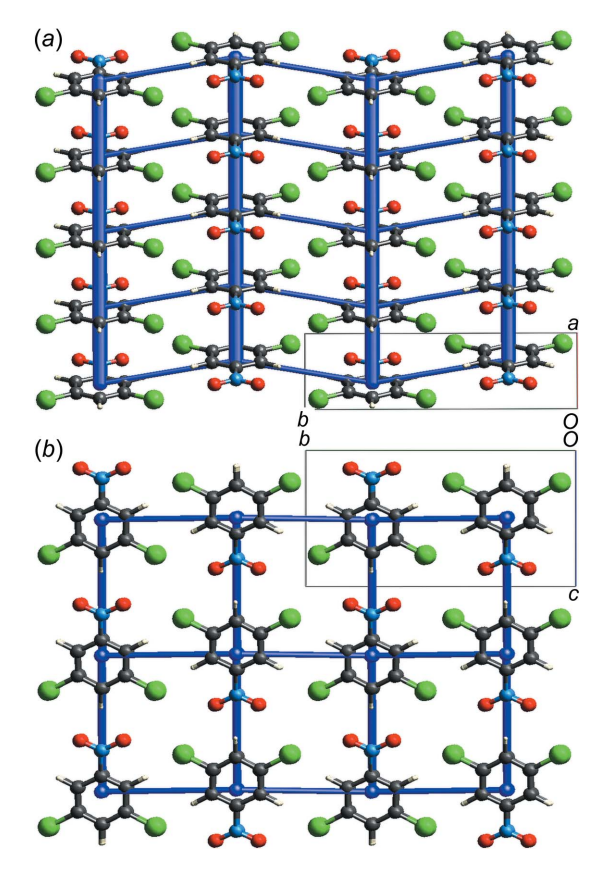


Figure 11 Two views of the total energy framework for structure (3), showing energies of interaction more cohesive than -8 kJ mol⁻¹ for clarity. (a) View along the c axis showing the dominant intermolecular interaction energy correlated with π -stacking and (b) view along the c axis with the intermolecular interaction energy correlated with the self-complementary $Cl\cdots O$ halogen bond shown horizontally parallel to the b axis, and the intermolecular interaction energy correlated with the bifurcated $C-H\cdots O$ (nitro) interaction shown vertical parallel to the c axis.

-and-conditions) on Wiley Online Library for rules of use; OA articles are governed by the applicable Creative Commons Licens

research papers

Figure 12 The search schemes used for (a) the self-complementary $C-X\cdots O$ halogen bond and (b) the bifurcated arene-nitrobenzene $C-H\cdots O$ interaction

van der Waals radii plus 0.15 Å maintaining the angle restraint resulted in 1757 hits in 1599 structures, suggesting that this interaction is a common interaction while not always identifiable as a close contact.

4. Conclusions

This systematic examination of close contacts and intermolecular interaction energies within the homologous series of 1,3-dihalo-5-nitrobenzenes demonstrates the importance of coupling close contacts with intermolecular energy calculations to better understand interactions within crystal structures. Overall, in these structures, the π -stacking interaction with a large dispersion component dominates. It is noteworthy that the strongest red coloration on the Hirshfeld surfaces of the three structures, corresponding to the closest contact, is a Type I iodine-iodine interaction in the structure of 1,3-diiodo-5-nitrobenzene and is weakly cohesive within the crystal. Furthermore, in these structures, it is reasonable to conclude that the size and nature of the halogen is a major factor in the relative interplay between the other close contacts observed. Thus the π -stacking interaction energy decreases as the size of the halogen atom decreases along with decreased surface area. Also, the self-complementary halogen · · · O(nitro) interaction weakens from iodine to chlorine in accord with the reduced σ -hole from iodine to chlorine (Fig. 7) coupled with a reduced dispersive component. Finally, while the overall intermolecular energy corresponding to the bifurcated C-H···O interaction decreases slightly from (1) to (3), this is a noticeably closer contact with (3), presumably due to the smaller atomic volume of the flanking Cl atoms.

Funding information

Funding for this research was provided by: National Science Foundation, Directorate for Mathematical and Physical Sciences (grant No. CHE-1903593).

References

Allen, F. H., Lommerse, J. P. M., Hoy, V. J., Howard, J. A. K. & Desiraju, G. R. (1997). *Acta Cryst.* B**53**, 1006–1016.

Awwadi, F. F., Willett, R. D., Peterson, K. A. & Twamley, B. (2006).
Chem. Eur. J. 12, 8952–8960.

Barbour, L. J. (2020). J. Appl. Cryst. 53, 1141-1146.

Bérubé, M. & Poirier, D. (2004). Org. Lett. 6, 3127-3130.

Bhar, A., Aune, J. P., Benali-Cherif, N., Benmenni, L. & Giorgi, M. (1995). *Acta Cryst.* C**51**, 256–260.

Bondi, A. (1964). J. Phys. Chem. 68, 441-451.

Bruker (2014). APEX2, SMART, SADABS, and SAINT. Bruker AXS Inc., Madison, Wisconsin, USA.

Bruno, I. J., Cole, J. C., Edgington, P. R., Kessler, M., Macrae, C. F., McCabe, P., Pearson, J. & Taylor, R. (2002). *Acta Cryst.* B58, 389–397.

Clark, T., Hennemann, M., Murray, J. S. & Politzer, P. (2007). J. Mol. Model. 13, 291–296.

Feng, Y., Chen, H., Liu, Z. X., He, Y. M. & Fan, Q. H. (2016). Chemistry, 22, 4980–4990.

Groom, C. R., Bruno, I. J., Lightfoot, M. P. & Ward, S. C. (2016). Acta Cryst. B72, 171–179.

Guillot, R. (2019). *CSD Communication* (CCDC deposition number 1895422). CCDC, Cambridge, England.

Ibrahim, M. A. A. & Moussa, N. A. M. (2020). ACS Omega, **5**, 21824–21835.

Ibrahim, M. A. A., Saeed, R. R. A., Shehata, M. N. I., Ahmed, M. N.,
Shawky, A. M., Khowdiary, M. M., Elkaeed, E. B., Soliman, M. E. S.
& Moussa, N. A. M. (2022). *Int. J. Mol. Sci.* 23, 3114.

Lim, J. Y. C., Cunningham, M. J., Davis, J. J. & Beer, P. D. (2015). Chem. Commun. 51, 14640–14643.

Mackenzie, C. F., Spackman, P. R., Jayatilaka, D. & Spackman, M. A. (2017). *IUCrJ*, **4**: 575–587.

Nemec, V. & Cinčić, D. (2016). CrystEngComm, 18, 7425-7429.

Nguyen, S. T., Rheingold, A. L., Tschumper, G. S. & Watkins, D. L. (2016). *Cryst. Growth Des.* **16**, 6648–6653.

Politzer, P. & Murray, J. S. (2013). ChemPlusChem, 14, 278-294.

Ramasubbu, N., Parthasarathy, R. & Murray-Rust, P. (1986). *J. Am. Chem. Soc.* **108**, 4308–4314.

Sheldrick, G. M. (2015a). Acta Cryst. A71, 3-8.

Sheldrick, G. M. (2015b). Acta Cryst. C71, 3-8.

Spackman, M. A. & Jayatilaka, D. (2009). CrystEngComm, 11, 19–32.
 Spackman, P. R., Turner, M. J., McKinnon, J. J., Wolff, S. K.,
 Grimwood, D. J., Jayatilaka, D. & Spackman, M. A. (2021). J. Appl. Cryst. 54, 1006–1011.

Thalladi, V. R., Goud, B. S., Hoy, V. J., Allen, F. H., Howard, J. A. K. & Desiraju, G. R. (1996). *Chem. Commun.* pp. 401–402.

Turner, M. J., Grabowsky, S., Jayatilaka, D. & Spackman, M. A. (2014). *J. Phys. Chem. Lett.* **5**, 4249–4255.

Turner, M. J., McKinnon, J. J., Wolff, S. K., Gromwood, D. J., Spackman, P. R., Jayatilaka, D. & Spackman, M. A. (2017). CrystalExplorer. Version 17.5. University of Western Australia. https://crystalexplorer.scb.uwa.edu.au/.

Wavefunction (2010). Spartan'10. Wavefunction Inc., Irvine, CA, USA. http://downloads.wavefun.com/.

Weegen, R. van der, Teunissen, A. J. P. & Meijer, E. W. (2017). *Chem. Eur. J.* **23**, 3773–3783.

s20532296, 2022, 10, Downloaded from https://onlinelibrary.wiley.com/doi/10.1107/S2053229622009275 by University Of Wisconsin - Sp. Wiley Online Library on [26/10/2023]. See the Terms

Acta Cryst. (2022). C78, 552-558 [https://doi.org/10.1107/S2053229622009275]

A structural and computational comparison of close contacts and related intermolecular energies of interaction in the structures of 1,3-diiodo-5-nitrobenzene, 1,3-dibromo-5-nitrobenzene, and 1,3-dichloro-5-nitrobenzene

Eric Bosch, Nathan P. Bowling and Erin D. Speetzen

Computing details

For all structures, data collection: *SMART* (Bruker, 2014); cell refinement: *SMART* (Bruker, 2014); data reduction: *SAINT* (Bruker, 2014); program(s) used to solve structure: SHELXT2018 (Sheldrick, 2015a); program(s) used to refine structure: *SHELXL2018* (Sheldrick, 2015b); molecular graphics: *X-SEED* (Barbour, 2020); software used to prepare material for publication: *X-SEED* (Barbour, 2020).

1,3-Diiodo-5-nitrobenzene (1)

Crystal data

 $C_6H_3I_2NO_2$ $M_r = 374.89$ Monoclinic, $P2_1/m$ a = 4.1810 (5) Å b = 15.0336 (17) Å c = 6.7970 (8) Å $\beta = 96.506$ (2)° V = 424.48 (9) Å³

Data collection

Z=2

Bruker APEX-I CCD diffractometer

Radiation source: fine-focus sealed tube

Graphite monochromator

Detector resolution: 8.3660 pixels mm⁻¹

phi and ω scans

Absorption correction: multi-scan (SADABS; Bruker, 2014) $T_{min} = 0.406$, $T_{max} = 0.746$

I min 0.100, I max 0.7

Refinement

Refinement on F^2 Least-squares matrix: full $R[F^2 > 2\sigma(F^2)] = 0.019$

 $wR(F^2) = 0.040$ S = 1.35

982 reflections 55 parameters

F(000) = 336

 $D_x = 2.933 \text{ Mg m}^{-3}$

Mo $K\alpha$ radiation, $\lambda = 0.71073$ Å Cell parameters from 4388 reflections

 $\theta = 2.7 - 27.2^{\circ}$

 $\mu = 7.36 \text{ mm}^{-1}$

T = 100 K

Trapezoidal, colourless

 $0.20 \times 0.20 \times 0.20 \text{ mm}$

5377 measured reflections 982 independent reflections 974 reflections with $I > 2\sigma(I)$

 $R_{\rm int} = 0.019$

 $\theta_{\text{max}} = 27.2^{\circ}, \ \theta_{\text{min}} = 2.7^{\circ}$

 $h = -5 \rightarrow 5$

 $k = -19 \rightarrow 19$

k = −19→1

 $l = -8 \rightarrow 8$

0 restraints

Primary atom site location: dual Hydrogen site location: inferred from

neighbouring sites

H-atom parameters constrained

 $w = 1/[\sigma^2(F_0^2) + 1.4021P]$

where $P = (F_0^2 + 2F_c^2)/3$

conditions) on Wiley Online Library for rules of use; OA articles are governed by the applicable Creative Commons Licensse

$$(\Delta/\sigma)_{\text{max}} = 0.001$$

 $\Delta\rho_{\text{max}} = 0.77 \text{ e Å}^{-3}$

$$\Delta \rho_{\min} = -0.75 \text{ e Å}^{-3}$$

Special details

Geometry. All esds (except the esd in the dihedral angle between two l.s. planes) are estimated using the full covariance matrix. The cell esds are taken into account individually in the estimation of esds in distances, angles and torsion angles; correlations between esds in cell parameters are only used when they are defined by crystal symmetry. An approximate (isotropic) treatment of cell esds is used for estimating esds involving l.s. planes.

Refinement. Single crystals of each were mounted on a Kryoloop using viscous hydrocarbon oil. Data were collected at 100 K using a Bruker Apex1 CCD diffractometer equipped with Mo K α radiation with $\lambda = 0.71073$ Å. Low temperature data collection was facilitated by use of a Kryoflex system with an accuracy of ± 1 K. Initial data processing was carried out using the Apex 2 software suite [Bruker, 2014]. Structures were solved using SHELXT-2018 (Sheldrick, 2015a) and refined against F2 using SHELXL-2018 (Sheldrick, 2015b). The program X-Seed was used as a graphical interface (Barbour, 2020).

Fractional atomic coordinates and isotropic or equivalent isotropic displacement parameters (\hat{A}^2)

	X	у	Z	$U_{ m iso}$ */ $U_{ m eq}$	
I1	0.83316 (5)	0.44977 (2)	0.22023 (3)	0.01726 (8)	
O1	0.2670 (7)	0.32177 (18)	0.8563 (4)	0.0290 (6)	
N1	0.3365 (10)	0.250000	0.7879 (6)	0.0166 (8)	
C1	0.5032 (11)	0.250000	0.6066 (7)	0.0138 (9)	
C2	0.5755 (8)	0.3312 (2)	0.5256 (5)	0.0145 (6)	
H2	0.524333	0.385788	0.585351	0.017*	
C3	0.7255 (8)	0.3296 (2)	0.3537 (5)	0.0139 (6)	
C4	0.8033 (11)	0.250000	0.2672 (7)	0.0150 (9)	
H4	0.908365	0.250000	0.150367	0.018*	

Atomic displacement parameters (Å²)

	U^{11}	U^{22}	U^{33}	U^{12}	U^{13}	U^{23}
I1	0.02045 (12)	0.01361 (12)	0.01868 (12)	-0.00068(8)	0.00633 (8)	0.00277 (8)
O1	0.0447 (17)	0.0197 (14)	0.0264 (14)	0.0007 (12)	0.0202 (12)	-0.0062 (11)
N1	0.017(2)	0.017(2)	0.0154 (19)	0.000	0.0019 (16)	0.000
C1	0.012(2)	0.018(2)	0.012(2)	0.000	0.0009 (17)	0.000
C2	0.0142 (15)	0.0134 (15)	0.0157 (15)	0.0008 (12)	0.0009 (12)	-0.0009 (12)
C3	0.0134 (14)	0.0120 (15)	0.0161 (15)	-0.0018 (12)	0.0009 (12)	0.0020 (12)
C4	0.012(2)	0.021(2)	0.012(2)	0.000	0.0019 (17)	0.000

Geometric parameters (Å, °)

I1—C3	2.094 (3)	C2—C3	1.388 (5)	
O1—N1	1.223 (3)	C2—H2	0.9500	
N1—C1	1.483 (6)	C3—C4	1.388 (4)	
C1—C2	1.387 (4)	C4—H4	0.9500	
C1—C2 ⁱ	1.387 (4)			
O1 ⁱ —N1—O1	123.9 (4)	C3—C2—H2	121.4	
O1 ⁱ —N1—C1	118.0 (2)	C4—C3—C2	121.5 (3)	
O1—N1—C1	118.0 (2)	C4—C3—I1	119.2 (2)	

C2—C1—C2 ⁱ	123.4 (4)	C2—C3—I1	119.3 (2)
C2—C1—N1	118.3 (2)	C3 ⁱ —C4—C3	119.1 (4)
C2i—C1—N1	118.3 (2)	C3 ⁱ —C4—H4	120.5
C1—C2—C3	117.2 (3)	C3—C4—H4	120.5
C1—C2—H2	121.4		

Symmetry code: (i) x, -y+1/2, z.

Hydrogen-bond geometry (Å, °)

<i>D</i> —H··· <i>A</i>	<i>D</i> —H	$H\cdots A$	D··· A	<i>D</i> —H··· <i>A</i>
C2—H2···I1 ⁱⁱ	0.95	3.25	4.172 (3)	165

Symmetry code: (ii) -x+1, -y+1, -z+1.

1,3-Dibromo-5-nitrobenzene (2)

Crystal data

 $C_6H_3Br_2NO_2$ F(000) = 264 $M_r = 280.91$ $D_{\rm x} = 2.455 \; {\rm Mg \; m^{-3}}$ Monoclinic, $P2_1/m$ Mo $K\alpha$ radiation, $\lambda = 0.71073 \text{ Å}$ a = 3.9721 (7) ÅCell parameters from 2304 reflections b = 14.164 (2) Å $\theta = 2.9 - 27.1^{\circ}$ $\mu = 10.61 \text{ mm}^{-1}$ c = 6.7971 (11) Å $\beta = 96.486 (2)^{\circ}$ T = 100 K $V = 379.97 (11) \text{ Å}^3$ Cut plate, colourless Z = 2 $0.38\times0.26\times0.09~mm$

Data collection

Bruker APEX-I CCD diffractometer Radiation source: fine-focus sealed tube Graphite monochromator Detector resolution: 8.3660 pixels mm⁻¹ phi and ω scans Absorption correction: multi-scan (SADABS; Bruker, 2014) $T_{\min} = 0.343$, $T_{\max} = 0.746$

Refinement

Refinement on F^2 Least-squares matrix: full $R[F^2 > 2\sigma(F^2)] = 0.029$ $wR(F^2) = 0.081$ S = 1.09874 reflections 55 parameters 0 restraints

Primary atom site location: dual

4446 measured reflections 874 independent reflections 764 reflections with $I > 2\sigma(I)$ $R_{\text{int}} = 0.044$ $\theta_{\text{max}} = 27.1^{\circ}, \ \theta_{\text{min}} = 2.9^{\circ}$ $h = -5 \rightarrow 5$ $k = -18 \rightarrow 18$ $l = -8 \rightarrow 8$

Hydrogen site location: inferred from neighbouring sites H-atom parameters constrained $w=1/[\sigma^2(F_o{}^2)+(0.0519P)^2]$ where $P=(F_o{}^2+2F_c{}^2)/3$ $(\Delta/\sigma)_{\rm max}=0.001$ $\Delta\rho_{\rm max}=1.04~{\rm e}~{\rm Å}^{-3}$ $\Delta\rho_{\rm min}=-0.52~{\rm e}~{\rm Å}^{-3}$

Special details

Geometry. All esds (except the esd in the dihedral angle between two l.s. planes) are estimated using the full covariance matrix. The cell esds are taken into account individually in the estimation of esds in distances, angles and torsion angles; correlations between esds in cell parameters are only used when they are defined by crystal symmetry. An approximate (isotropic) treatment of cell esds is used for estimating esds involving l.s. planes.

Refinement. Single crystals of each were mounted on a Kryoloop using viscous hydrocarbon oil. Data were collected at 100 K using a Bruker Apex1 CCD diffractometer equipped with Mo K α radiation with $\lambda = 0.71073$ Å. Low temperature data collection was facilitated by use of a Kryoflex system with an accuracy of ± 1 K. Initial data processing was carried out using the Apex 2 software suite [Bruker, 2014]. Structures were solved using SHELXT-2018 (Sheldrick, 2015a) and refined against F2 using SHELXL-2018 (Sheldrick, 2015b). The program X-Seed was used as a graphical interface (Barbour, 2020).

Fractional atomic coordinates and isotropic or equivalent isotropic displacement parameters (\hat{A}^2)

	x	У	z	$U_{ m iso}$ */ $U_{ m eq}$	
Br1	0.84325 (8)	0.55011 (2)	0.22435 (5)	0.02091 (17)	
O1	0.2977 (7)	0.67372 (17)	0.8585 (4)	0.0301 (6)	
N1	0.3658 (10)	0.750000	0.7878 (7)	0.0198 (9)	
C2	0.6006(8)	0.6637(2)	0.5205 (5)	0.0175 (7)	
H2	0.550372	0.605683	0.581154	0.021*	
C3	0.7459 (8)	0.6659(2)	0.3462 (6)	0.0171 (7)	
C1	0.5304 (11)	0.750000	0.6038 (7)	0.0169 (9)	
C4	0.8204 (11)	0.750000	0.2566 (8)	0.0212 (11)	
H4	0.920583	0.750000	0.136165	0.025*	

Atomic displacement parameters (\mathring{A}^2)

	U^{11}	U^{22}	U^{33}	U^{12}	U^{13}	U^{23}
Br1	0.0237 (3)	0.0141 (2)	0.0254 (3)	0.00110 (11)	0.00482 (17)	-0.00274 (12)
O1	0.0464 (16)	0.0191 (12)	0.0271 (15)	-0.0050(12)	0.0135 (13)	0.0044 (11)
N1	0.021(2)	0.018(2)	0.019(2)	0.000	-0.0016 (16)	0.000
C2	0.0163 (15)	0.0153 (14)	0.0197 (18)	-0.0004(12)	-0.0030(13)	-0.0006(13)
C3	0.0130 (14)	0.0127 (15)	0.0246 (19)	0.0015 (11)	-0.0024(13)	-0.0037(13)
C1	0.014(2)	0.020(2)	0.016(2)	0.000	-0.0011 (19)	0.000
C4	0.015(2)	0.028 (3)	0.021 (3)	0.000	0.002(2)	0.000
	` ′	• • •	` '		` '	

Geometric parameters (Å, °)

Br1—C3	1.897 (3)	C2—C1	1.389 (4)
O1—N1	1.225 (3)	C2—H2	0.9500
N1—C1	1.475 (6)	C3—C4	1.385 (4)
C2—C3	1.375 (5)	C4—H4	0.9500
O1 ⁱ —N1—O1	123.8 (4)	C4—C3—Br1	119.2 (3)
O1 ⁱ —N1—C1	118.1 (2)	C2 ⁱ —C1—C2	123.4 (5)
O1—N1—C1	118.1 (2)	C2 ⁱ —C1—N1	118.3 (2)
C3—C2—C1	117.0 (3)	C2—C1—N1	118.3 (2)
C3—C2—H2	121.5	C3 ⁱ —C4—C3	118.7 (5)
C1—C2—H2	121.5	C3 ⁱ —C4—H4	120.7

120.7

C2—C3—C4	122.0(3)	C3—C4—H4	
C2—C3—Br1	118.9 (2)		

Symmetry code: (i) x, -y+3/2, z.

Hydrogen-bond geometry (Å, °)

<i>D</i> —H··· <i>A</i>	<i>D</i> —H	$H\cdots A$	D··· A	<i>D</i> —H··· <i>A</i>
C2—H2···Br1 ⁱⁱ	0.95	3.09	3.997 (3)	161

Symmetry code: (ii) -x+1, -y+1, -z+1.

1,3-Dichloro-5-nitrobenzene (3)

Crystal data

F(000) = 192
$D_{\rm x} = 1.783 \; {\rm Mg \; m^{-3}}$
Mo $K\alpha$ radiation, $\lambda = 0.71073 \text{ Å}$
Cell parameters from 2128 reflections
$\theta = 3.0-26.9^{\circ}$
$\mu = 0.85 \text{ mm}^{-1}$
T = 100 K
Cut rod, colourless
$0.37\times0.13\times0.03~mm$

Data collection

Bruker APEX-I CCD	4560 measured reflections
diffractometer	813 independent reflections
Radiation source: fine-focus sealed tube	747 reflections with $I > 2\sigma(I)$
Graphite monochromator	$R_{\rm int} = 0.021$
Detector resolution: 8.3660 pixels mm ⁻¹	$\theta_{\rm max} = 27.1^{\circ}, \theta_{\rm min} = 3.0^{\circ}$
phi and ω scans	$h = -4 \longrightarrow 4$
Absorption correction: multi-scan	$k = -17 \rightarrow 17$
(SADABS; Bruker, 2014)	$l = -8 \longrightarrow 8$
$T_{\rm min} = 0.702$, $T_{\rm max} = 0.746$	

Refinement

Refinement on F^2 Least-squares matrix: full	Hydrogen site location: inferred from neighbouring sites
$R[F^2 > 2\sigma(F^2)] = 0.028$	H-atom parameters constrained
$wR(F^2) = 0.071$	$w = 1/[\sigma^2(F_0^2) + (0.0398P)^2 + 0.1267P]$
S = 1.12	where $P = (F_0^2 + 2F_c^2)/3$
813 reflections	$(\Delta/\sigma)_{\rm max} < 0.001$
55 parameters	$\Delta ho_{ m max} = 0.37 \ m e \ \AA^{-3}$
0 restraints	$\Delta \rho_{\min} = -0.21 \text{ e Å}^{-3}$
Primary atom site location: dual	

Special details

Geometry. All esds (except the esd in the dihedral angle between two l.s. planes) are estimated using the full covariance matrix. The cell esds are taken into account individually in the estimation of esds in distances, angles and torsion angles; correlations between esds in cell parameters are only used when they are defined by crystal symmetry. An approximate (isotropic) treatment of cell esds is used for estimating esds involving l.s. planes.

and-conditions) on Wiley Online Library for rules of use; OA articles are governed by the applicable Creative Commons License

Refinement. Single crystals of each were mounted on a Kryoloop using viscous hydrocarbon oil. Data were collected at 100 K using a Bruker Apex1 CCD diffractometer equipped with Mo K α radiation with $\lambda = 0.71073$ Å. Low temperature data collection was facilitated by use of a Kryoflex system with an accuracy of ± 1 K. Initial data processing was carried out using the Apex 2 software suite [Bruker, 2014]. Structures were solved using SHELXT-2018 (Sheldrick, 2015a) and refined against F2 using SHELXL-2018 (Sheldrick, 2015b). The program X-Seed was used as a graphical interface (Barbour, 2020).

Fractional atomic coordinates and isotropic or equivalent isotropic displacement parameters (\hat{A}^2)

	x	У	Z	$U_{ m iso}$ */ $U_{ m eq}$	
Cl1	0.86115 (10)	0.44740 (3)	0.23313 (5)	0.02154 (16)	
O1	0.3346 (3)	0.32913 (8)	0.86816 (17)	0.0290(3)	
N1	0.3994 (5)	0.250000	0.7954(3)	0.0179 (4)	
C4	0.8446 (5)	0.250000	0.2540(3)	0.0174 (4)	
H4	0.942848	0.250000	0.131693	0.021*	
C1	0.5603 (5)	0.250000	0.6076 (3)	0.0153 (4)	
C3	0.7716 (4)	0.33764 (10)	0.3448 (2)	0.0163 (3)	
C2	0.6269 (4)	0.33974 (11)	0.5237 (2)	0.0162 (3)	
H2	0.576278	0.399770	0.585345	0.019*	

Atomic displacement parameters (\mathring{A}^2)

	U^{11}	<i>U</i> ²²	U^{33}	I /12	U^{13}	U^{23}
	U	U	U	U	0	<i>U</i> -
C11	0.0264(2)	0.0150(2)	0.0240(2)	-0.00205 (13)	0.00686 (15)	0.00304 (13)
O1	0.0442 (8)	0.0215 (6)	0.0230(6)	0.0070 (5)	0.0124 (5)	-0.0011(5)
N1	0.0167 (9)	0.0216 (9)	0.0154 (9)	0.000	0.0010(6)	0.000
C4	0.0143 (10)	0.0213 (11)	0.0165 (10)	0.000	0.0014(8)	0.000
C1	0.0128 (9)	0.0200 (10)	0.0131 (9)	0.000	0.0010(7)	0.000
C3	0.0141 (7)	0.0150(7)	0.0194 (7)	-0.0019(5)	0.0000 (5)	0.0020(6)
C2	0.0144 (7)	0.0161(7)	0.0178 (7)	0.0000(5)	-0.0001(5)	-0.0017(6)

Geometric parameters (Å, °)

C11—C3	1.7306 (15)	C4—H4	0.9500
O1—N1	1.2242 (14)	C1—C2 ⁱ	1.3864 (17)
N1—C1	1.477 (3)	C1—C2	1.3865 (17)
C4—C3i	1.3885 (18)	C3—C2	1.392 (2)
C4—C3	1.3885 (18)	C2—H2	0.9500
01—N1—01 ⁱ	123.75 (18)	C2—C1—N1	117.96 (10)
O1—N1—C1	118.12 (9)	C4—C3—C2	121.72 (14)
O1 ⁱ —N1—C1	118.12 (9)	C4—C3—C11	119.39 (12)
C3 ⁱ —C4—C3	118.91 (19)	C2—C3—C11	118.89 (11)
C3 ⁱ —C4—H4	120.5	C1—C2—C3	116.80 (14)
C3—C4—H4	120.5	C1—C2—H2	121.6
C2 ⁱ —C1—C2	124.05 (19)	C3—C2—H2	121.6
C2i—C1—N1	117.96 (10)		

Symmetry code: (i) x, -y+1/2, z.